ORIGINAL PAPER

A Simplified pulse-coupled neural network for adaptive segmentation of fabric defects

**Meihong Shi · Shoushan Jiang · Huiran Wang ·
Bugao Xu**

Abstract This paper describes an adaptive image-segmentation method based on a simplified pulse-coupled neural network (PCNN) for detecting fabric defects. Defect segmentation has been a focal point in fabric inspection research, and it remains challenging because it detects delicate features of defects complicated by variations in weave textures and changes in environmental factors (e.g., illumination, noise). A new parameter called the deviation of the contrast (DOC) was introduced to describe the contrast difference in row and column between the analyzed image and a defect-free image of the same fabric. The DOC essentially weakens the influence of the weave texture and the illumination. The simplification of PCNN reduces the number of the network's parameters by utilizing the local and global DOC information for the parameter selections. The validation tests on the developed algorithms were performed with fabric images captured by a line-scan camera on an inspection machine, and with images from TILDA's Textile Texture Database (http://lmb.informatik.uni-freiburg.de/research/dfg-texture/tilda) as well.

1 Introduction

Defect inspection is a vital step for quality assurance in fabric production. To improve the efficiency and reliability

M. Shi · S. Jiang · H. Wang
School of Computer Science, Xi'an Polytechnic University,
Xi'an 710048, People's Republic of China

B. Xu (✉)
Department of Human Ecology, University of Texas at Austin,
Austin, TX 78712, USA
e-mail: bxu@mail.utexas.edu

of fabric inspection, computer vision technology has been increasingly applied to detect and classify fabric defects automatically to replace the hand-counting method [1–4]. Image segmentation is the key to automatic detection of fabric defects. The texture and shape features of fabric defects can be extracted in the spatial domain using methods such as gray concurrence matrix, Markov random fields and mathematical morphology, ICA, and textural models, and then they can be classified using preset thresholds or artificial neural networks [5–9]. Fabric images can also be transformed to other domains using the fast Fourier transform, the Gabor transform, or the wavelet transform for locating defects in the images [10,11]. Of these methods, the wavelet transform appears more efficient and reliable for fabric defect detection, because it is more suitable than other transforms for analyzing localized features [10–13]. A PCNN-based method was also developed for defect segmentation [14]. However, most of these computer vision methods are limited to analyzing certain types of defects or lack flexibility in dealing with changes in fabric structures and background.

The study presented in this paper was in continuation of the PCNN development for improving its reliability in detecting fabric defects. A new defect descriptor was defined to measure the contrasts of adjacent rows and columns by comparing features in defective images with those in a defect-free image of the same fabric, which can undermine the effects of fabric textures and background noise. The previously used PCNN was also simplified to make it more computationally efficient and reliable in parameter selections.

2 Feature description of fabric images

The common causes of fabric defects are yarn faults, marks, and irregular interlacing of wefts and warps. In a defect-free

fabric, wefts and warps are regularly woven to form a period structure, and the corresponding image exhibits uniformly distributed patterns. On the other hand, a defective fabric often displays irregular textures, thus yielding disturbances in its uniform distributions. It is unreliable, however, to identify defects directly from the assessment of grayscale irregularity because the environmental factors (e.g., illumination, noise) and the weave textures can alter the image intensity appreciably. It is beneficial to use a defect-free image of the same fabric as a reference for identifying defects in defective images to undermine the influence of the overall texture of the fabric and the illumination. A fabric defect often occurs at a location where there is a sudden direction change between adjacent yarns. A descriptor to describe this phenomenon can be defined based on the grayscale contrasts of adjacent rows and columns. To make the defect detection adaptive to local grayscale variations, the contrast calculations will be limited to a small moving window. The algorithm is detailed as follows.

(1) Divide the $M \times N$ image into non-overlapping 3×3 windows, then compute the maximum, minimum, and median values of grayscales for each row and column in all of the windows. These statistical data are denoted as $r_{max}, r_{min}, r_{med}, c_{max}, c_{min}$, and c_{med}, respectively.

(2) Calculate four contrast parameters for each window by comparing the minimum and median values to the maximums, i.e.,

$$
\begin{aligned}
r_{kl}^1 &= \frac{r_{min}}{r_{max}} \\
r_{kl}^2 &= \frac{r_{med}}{r_{max}} \\
c_{kl}^1 &= \frac{c_{min}}{c_{max}} \\
c_{kl}^2 &= \frac{c_{med}}{c_{max}}
\end{aligned}
\tag{1}
$$

where $k = 1, 2, \ldots, M/3$ and $l = 1, 2, \ldots, N/3$.

(3) Select a defect-free image, and compute the same contrast parameters, denoted as r^1, r^2, c^1, and c^2, respectively.

(4) For the window at the kth row and lth column, a parameter g_{kl} is defined as:

$$
g_{kl} = \frac{|r_{kl}^1 - r^1|}{r^1} + \frac{|r_{kl}^2 - r^2|}{r^2} + \frac{|c_{kl}^1 - c^1|}{c^1} + \frac{|c_{kl}^2 - c^2|}{c^2}.
\tag{2}
$$

g_{kl} measures the localized deviation of the contrast (DOC) of a fabric image from a defect-free image of the same fabric. Once all $g_{k,l}$ are calculated, a DOC image with the dimension of $K \times L = M/3 \times N/3$,

can be generated. Because most of fabric defects have linear shapes oriented in the warp (vertical) or weft (horizontal) direction, the DOC can be summed up in row or in column to acquire the cumulative effect of a defect. A DOC curve in row or column will explicitly exhibit defects aligned in the perpendicular direction. Figure 1 shows the DOC curves of nine typical defects, in which the x coordinates indicate the positions (row or column) of the original image and the y coordinates denote the cumulative DOC values in rows or columns. The significant peaks of the curve unambiguously reveal defects out of the background.

3 Simplification of PCNN

3.1 PCNN's principle for image segmentation

A PCNN model originated from the explanation of the featured synchronization behavior observed experimentally in the visual cortex of a cat's brain [15]. In contrast to a traditional artificial neuron model, PCNN has distinctive characteristics. It transforms space information into temporal information in phase by switching the relative active phase among neurons corresponding to a series of binary images containing objectives, edges, and textures in image processing. These images have proven to be highly effective in research areas of image segmentation [16]. The main features of a PCNN [15,16] include, (1) each neuron outputs a dynamic pulse, (2) the network synchronizes the pulsing of neurons with similar external stimulus and spatial proximity, and (3) the network can be self adaptive to the varying external stimuli without being trained.

In a PCNN, the iterations at neuron N_{ij} can be expressed as follows:

$$
\begin{aligned}
F_{ij}[n] &= S_{ij} \\
L_{ij}[n] &= V_L \sum_{kl} w_{ijkl} Y_{kl}[n-1] \\
U_{ij}[n] &= F_{ij}[n](1 + \beta L_{ij}[n]) \\
Y_{ij}[n] &= \begin{cases} 1 & U_{ij}[n] \geq \theta_{ij}[n] \\ 0 & \text{otherwise} \end{cases} \\
\theta_{ij}[n] &= e^{(-t/\tau_\theta)} \theta_{ij}[n-1] - V_\theta Y[n]
\end{aligned}
\tag{3}
$$

where n is the number of iteration, S_{ij} is an external stimulus from the feeding field, L_{ij} is a regionally linking stimulus of its adjacent neurons N_{kl} from the coupling field, and $\sum_{kl} w_{ijkl}$ is a weight matrix of the interconnection. U_{ij} is the product of a feeding input F_{ij} and a shifted coupling input $(1 + \beta L_{ij})$, where β is a coefficient adjusting the strength of the linking. θ_{ij} is a time-dependant threshold that exponentially decreases with a time constant τ_θ. When U_{ij} exceeds θ_{ij}, the output Y_{ij} of N_{ij} is "1" or "pulsing," otherwise, it
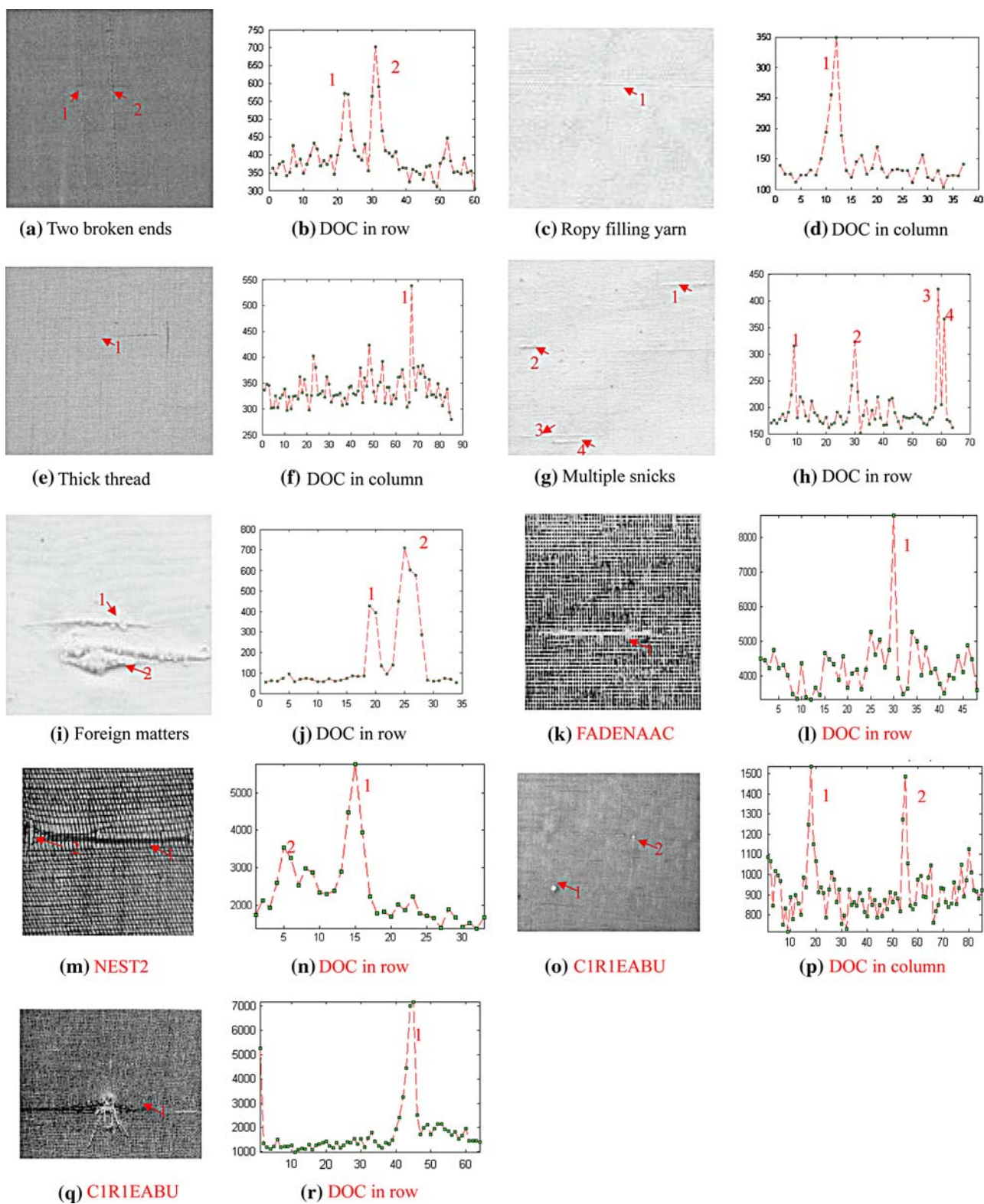
Fig. 1 DOC curves of various defects (images **k–q** are selected from the TILDA database)

is "0" or "not pulsing." Obviously, the "pulsing" time of Y_{ij} depends on not only on S_{ij} but also on β, τ_θ, w_{ijkl}, and the magnifying constants V_L and V_θ.

For a two-dimensional image of $M \times N$, the PCNN can have $M \times N$ input neurons, each corresponding to a pixel in the image and taking its grayscale as the external stimulus.

When $\beta = 0$, it means that the neurons are isolated rather than regionally coupled to one another. N_{ij} only receives external stimulus S_{ij}, and it pulses naturally at $t = \tau_\theta \ln \frac{V_\theta}{S_{ij}}$. After being reset, N_{ij} pulses again due to the influence of the external stimuli alone. The phenomenon continues, and each neuron pulses periodically at a frequency of $1/t$. Neurons pulsing at the same time (which is called synchronous pulsing) have the same external stimulus, and neurons pulsing at different times (which is called asynchronous pulsing) have different external stimuli. This leads to a binary segmentation of the processed image. When $\beta \neq 0$, it means that the neurons are regionally coupled, and a pulsing neuron N_{kl} produces a linking stimulus L_{ij} to a non-pulsing neuron N_{ij} as long as they are mutually coupled. The internal activation of N_{ij} is elevated to $S_{ij}(1 + \beta L_{ij})$ and will be caused to generate pulsing, which is called captured pulsing. These captured pulsing neurons will also lead other coupled neurons to pulse, a phenomenon that leads to signal spreading based on spatial proximity and external stimulus similarity and that produces synchronous bursts of pulses in PCNN. As a result of pulse coupling, neurons corresponding to the pixels that are in the same region and have the same grayscale tend to pulse synchronously, and near and similar pixels are more likely to be captured and then forced to pulse concurrently. This inherent characteristic of PCNN lends itself as one of most effective segmentation methods. Apparently, the effectiveness of PCNN segmentation also relies on the parameters used in the network, such as V_θ, V_L, w_{ijkl}, β and τ_θ. The selections and adjustments of these parameters often make proper image segmentation unreliable.

3.2 Simplified PCNN model and parameter descriptions

To simplify the PCNN model for this application, we modified the input–output iterations as follows:

$$
\begin{aligned}
F_{ij}[n] &= S_{ij} \\
L_{ij}[n] &= \sum_{k,l=-1}^{+1} w_{ijkl} Y_{kl}[n-1] \\
U_{ij}[n] &= F_{ij}[n](1 + \beta_{ij} L_{ij}[n]) \\
Y_{ij}[n] &= \text{step}(U_{ij}[n] - \theta_{ij}[n]) \\
\theta_{ij}[n] &= \theta_{ij}[n-1] - \Delta\theta
\end{aligned}
\qquad (4)
$$

(1) L_{ij} only receives the outputs from the coupled neurons in the 3×3 linking field. The connection weight w_{ijkl} is determined only by the external stimuli in the window, i.e., $w_{ijkl} = \frac{1 - |S_{ij} - S_{kl}|}{|i-k| + |j-l|}$. This means that for two neurons N_{ij} and N_{kl} in the same window, the smaller their spatial distance, and the smaller the difference between their external stimuli, the larger is the weight coefficient w_{ijkl}, and the easier it is to have synchronous pulsing.

(2) The linking coefficient β_{ij} is now related to the external stimulus, i.e., $\beta_{ij} = \frac{1}{e^{\lambda \times |S_{ij} - M|}}$, where λ is a coefficient that is inversely proportional to the contrast of a non-defective image, and that is used to modulate the duration of the neuron pulsing. M is the average external stimulus of the currently pulsed neurons in the net, and β_{ij} can be used to excite or inhibit N_{ij} to pulse synchronously with the pulsing neurons.

(3) θ_{ij} is a dynamic threshold that is linearly decreased with a constant $\Delta\theta = \frac{k \times \bar{g}}{\bar{g}_{normal}}$, where $\bar{g}$ and $\bar{g}_{normal}$ are the averages of the DOC of an image and its corresponding non-defective image, and k is a constant (it was set to 5). The larger the rate $\frac{\bar{g}}{\bar{g}_{normal}}$, the larger the decay of the pulsing threshold θ_{ij}.

(4) Initial threshold $\theta[0]$ can directly influence the iteration speed and segmentation quality. A lower $\theta[0]$ can improve the speed, but may cause underestimation of defects. We chose the following equation to calculate the initial threshold: $\theta[0] = \frac{g_{max\_normal} + g_{max}}{2}$, where g_{max} and g_{max_normal} are the maximum DOCs of an image and its corresponding non-defective image.
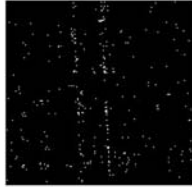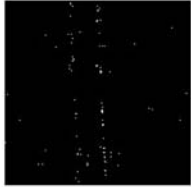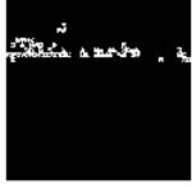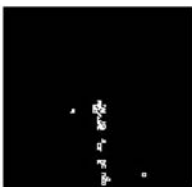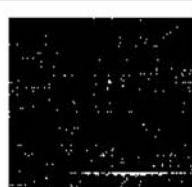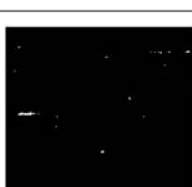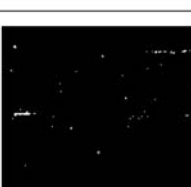
In the above-described simplified PCNN model, several former parameters are reduced to two parameters: β_{ij} and $\Delta\theta$, and their values are adjusted based on the DOC data and spatial distribution of the external stimuli. As a result, the segmented image tends to have a similar appearance to the original image.

4 Experiment results and discussion

The sample images consisted of the fabric image taken by a line-scan CCD camera and the images chosen from the TILDA database [17], and the image analysis was implemented on the VC++ platform. The line-scan camera has a 2,048 sensor array, and was mounted on a fabric inspection machine where it had a resolution of 0.2 mm/pixel (approximately 125 DPI). Hence, the camera's transverse coverage was about 410 mm. The lighting source was a regular fluorescent light on the inspection machine. The weave structures and the image capture conditions of the images in the TILDA were unknown, and they were used to demonstrate if the proposed algorithm is able to segment defects out of images that differ in textures, resolutions, and lighting conditions.

Table 1 compares the segmentation results of the simplified PCNN method discussed above, the Otsu method [18], and the regular PCNN method [15] on a number of common fabric defects. Each defective image was mixed with 10% random noise. When defective images are visually distinctive, all the three methods can detect defects well (see foreign

Table 1 Segmentation of different fabric defects with various methods[a]

	Original	Simplified PCNN	Otsu	Regular PCNN
Broken ends 256×256				
Ropy filling 256×256				
Loose warp 256×256				
Single snick 256×256				
Multiple snick 256×256				
Foreign matter 256×256				
Oily stain 256×256				

matter and oily stain defects), but when defects are not so sharp, only the simplified PCNN method is robust enough to find them reasonably well and to suppress the background noise with extracted defects being complete and clean. The other two methods seem to underestimate the defects and overestimate the noise in some defective images.

Table 1 continued

[a] The last ten defect images are from the TILDA database

In order to quantitatively evaluate the performance of the simplified PCNN method, we used a composite index J to measure the quality of image segmentation in [19].

$$J = UM \times C \times SM \times (1 - D) \tag{5}$$

where UM, C, SM, and D are the uniformity measure, contrast, shape measure, and degree of fuzziness of segmented objects, respectively. Table 2 presents these performance parameters of the three segmentation methods for the same defective images in Table 1. The individual parameters of a segmentation method rely on the criterion used in the method. If a parameter is defined in a way consistent with the criterion, the performance of the method on this parameter will be optimal [20]. Although different segmentation methods

Table 2 Comparison of the performance evaluation of the three methods

Defective images	Segmentation methods	UM	C	SM	D	J
Broken ends	Simplified PCNN	0.9756	0.6419	0.4681	0.5170	0.1416
	Otsu	0.9830	0.5190	0.9179	0.8655	0.0630
	Regular PCNN	0.9786	0.5931	0.5296	0.6101	0.1198
Ropy filling	Simplified PCNN	0.9880	0.6063	0.2841	0.1883	0.1381
	Otsu	0.9907	0.5456	0.4599	0.7717	0.0567
	Regular PCNN	0.9894	0.5536	0.3947	0.4168	0.1261
Loose warp	Simplified PCNN	0.9959	0.8207	0.1291	0.6045	0.0417
	Otsu	0.9964	0.6012	0.1757	0.8904	0.0115
	Regular PCNN	0.9963	0.6302	0.1562	0.8440	0.0153
Single snick	Simplified PCNN	0.9922	0.6447	0.2486	0.5802	0.0668
	Otsu	0.9926	0.6074	0.2814	0.7971	0.0344
	Regular PCNN	0.9924	0.6192	0.2774	0.6534	0.0591
Multiple snick	Simplified PCNN	0.9874	0.6916	0.4782	0.6415	0.1171
	Otsu	0.9887	0.6650	0.5102	0.7825	0.0730
	Regular PCNN	0.9887	0.6650	0.5102	0.7201	0.0939
Foreign matter	Simplified PCNN	0.9974	0.8639	0.4890	0.7103	0.1094
	Otsu	0.9974	0.8639	0.4890	0.7507	0.1050
	Regular PCNN	0.9972	0.8622	0.4865	0.6325	0.1053
Oily stain	Simplified PCNN	0.9944	0.6825	0.3503	0.6405	0.0855
	Otsu	0.9948	0.6724	0.3455	0.7694	0.0533
	Regular PCNN	0.9946	0.6619	0.3012	0.5571	0.0878
C1R1EAEH	Simplified PCNN	0.9982	0.5474	0.5727	0.8566	0.0449
	Otsu	0.6925	0.5731	0.7028	0.8682	0.0368
	Regular PCNN	0.4648	0.5910	0.3517	0.8885	0.0108
C1R1EAEM	Simplified PCNN	0.7557	0.6056	0.4040	0.7723	0.0421
	Otsu	0.5785	0.4804	0.6600	0.8616	0.0254
	Regular PCNN	0.6358	0.5769	0.1318	0.4724	0.0255
C1R1EAEC	Simplified PCNN	0.8324	0.6006	0.4324	0.8041	0.0423
	Otsu	0.5402	0.5713	0.5927	0.8856	0.0209
	Regular PCNN	0.3543	0.6665	0.2650	0.6540	0.0217
C1R1EADI	Simplified PCNN	0.7305	0.7092	0.4349	0.3065	0.1563
	Otsu	0.4957	0.6506	0.4789	0.9165	0.0129
	Regular PCNN	0.3460	0.7286	0.1012	0.4208	0.0148
C1R1EAJA	Simplified PCNN	0.5244	0.7371	0.1193	0.6095	0.0180
	Otsu	0.3612	0.5117	0.3233	0.9208	0.0047
	Regular PCNN	0.1821	0.8468	0.0886	0.3550	0.0088
C1R1EAMT	Simplified PCNN	0.4417	0.7471	0.1618	0.7767	0.0119
	Otsu	0.2173	0.6839	0.1556	0.9138	0.0020
	Regular PCNN	0.3148	0.6387	0.1327	0.8923	0.0029

Table 2 continued

Defective images	Segmentation methods	UM	C	SM	D	J
FADENAAC	Simplified PCNN	0.8696	0.4585	0.3761	0.6821	0.0477
	Otsu	0.3173	0.4721	0.3317	0.7525	0.0123
	Regular PCNN	0.7115	0.4981	0.2679	0.6124	0.0368
NEST2	Simplified PCNN	0.5356	0.6618	0.1310	0.4239	0.0268
	Otsu	0.3729	0.5882	0.2039	0.8409	0.0071
	Regular PCNN	0.1610	0.8324	0.0595	0.6198	0.0030
C1R1EABU	Simplified PCNN	0.3170	0.8324	0.7310	0.9585	0.0080
	Otsu	0.1052	0.8275	0.0654	0.9451	0.0003
	Regular PCNN	0.2170	0.8324	0.0731	0.9585	0.0005
HAFT1	Simplified PCNN	0.9720	0.6575	0.3515	0.6990	0.0676
	Otsu	0.4267	0.6301	0.3627	0.8501	0.0146
	Regular PCNN	0.6309	0.6575	0.2695	0.5463	0.0507

exhibit different rankings in these performance parameters when applied to different defective images, the overall performance measure J of the simplified PCNN is superior to those of the other two methods.

5 Conclusion

This paper discusses the methods that describe the features of fabric defects and perform defect segmentation from various texture backgrounds using a simplified PCNN. The contrast of fabric defects can be enhanced and the influence of weave textures can be weakened by referencing the features of a defect-free image of the same fabric. The contrast comparison between a defective image and a defect-free image is implemented in a moving window, and reflected by a new parameter called as the deviation of the contrast (DOC). The simplified PCNN needs only two parameters that can be adaptively adjusted based on local and global characteristics of the image. Both the visual assessments and quantitative data of the images taken from a line-scan camera and the images from the TILDA database prove the simplified PCNN method to be effective and robust for defect segmentation.

References

1. Li, L.Q., Huang, X.B.: Recent studies on image-based automatic fabric inspection system. J. DongHua Univ. **28**(4), 118–122 (2002)
2. Conci, A., Procenca, C.B.: A comparison between image-processing approaches to textile inspection. J. Textile Inst. **91**(2), 317–323 (2000)
3. Kuo, C.F., Lee, C.J., Tsai, C.C.: Using a neural network to identify fabric defects in dynamic cloth inspection. Textile Res. J. **73**(3), 238–244 (2003)
4. Chen, J.J., Xie, C.P.: Fabric detection technique based on neural network. Textile Res. J. **27**(4), 36–39 (2006)
5. Zhang, Y.F., Bresee, R.R.: Fabric defect detection and classification using image analysis. Textile Res. J. **65**(1), 1–9 (1995)
6. Chetverikov, D., Hanbury, A.: Finding defects in texture using regularity and local orientation. Pattern Recogn. **35**, 203–218 (2002)
7. Sezer, O.G., ErtEE, A., Eril, A.: Using perceptual relation of regularity and anisotropy in the texture with independent components for defect detection. IEEE Pattern Recogn. **40**(1), 121–133 (2007)
8. Cohen, F.S., Fan, Z., Attali, S.: Automated inspection of textile fabrics using textural models. IEEE Trans. Pattern Anal. Machine Intell. **3–8**, 803–808 (1991)
9. Meylani, R.: 2-D Iteratively reweighted least squares lattice algorithm and its application to defect detection in textured images. EIEICE Trans. Fundam. Electron. Communi. Computer Sci. E **89**(A5), 1484–1494 (2006)
10. Jasper, W.J., Potlapalli, H.: Image analysis of mispicks in woven fabric. Textile Res. J. **65**(11), 683–692 (1995)
11. Jasper, W.J., Gamier, S.J., Potlapalli, H.: Texture characterization and defect detection using adaptive wavelets. Optical Eng. **35**(11), 3140–3149 (1996)
12. Fusheng, Y.: Engineering Analysis and Application based on Wavelet Transform. pp. 32–69. Science Press, Beijing (2000)
13. Li, L.Q., Huang, X.B.: Woven fabric defect detection with features based on adaptive wavelets. J. DongHua Univ. **27**(4), 82–87 (2001)
14. Shi, M.H., Zhang, J.Y.: Fabric's defect detection based on improved PCNN. Silk **6**, 14–17 (2002)
15. Johnson, J.L., Padgett, M.L.: PCNN models and applications. IEEE Trans. Neural Netw. **10**(3), 80–498 (1999)
16. Kuntimad, G., Ranganath, H.S.: Perfect image segmentation using pulse-coupled neural networks. IEEE Trans. Neural Netw. **10**(3), 591–598 (1999)
17. Workgroup on Texture Analysis of DFG. TILDA Textile Texture Database: http://lmb.informatik.uni-freiburg.de/research/dfg-texture/tilda
18. Liu, J.Z., Li, W.Q.: The automatic thresholding of gray-level pictures via two-dimensional Otsu method. Acta Automat. Sinica **19**(1), 101–105 (1993)
19. Ge-xian, H., Du-yan, B.: Evaluation methods for image segmentation. J. Image Graph. **5**(1), 39–43 (2000)
20. Zhang, Y.J.: Image Segmentation. pp. 149–169. Science Press, Beijing (2001)